Geophysical Research Letters

RESEARCH LETTER
10.1029/2019GL085667

Southern Annular Mode Influence on Wintertime Ventilation of the Southern Ocean Detected in Atmospheric O_2 and CO_2 Measurements

Cynthia D. Nevison[1], David R. Munro[2,3], Nicole S. Lovenduski[1,4], Ralph F. Keeling[5], Manfredi Manizza[5], Eric J. Morgan[5], and Christian Rödenbeck[6]

[1]Institute of Arctic and Alpine Research, University of Colorado, Boulder, CO, USA, [2]Cooperative Institute for Research in Environmental Sciences, University of Colorado, Boulder, CO, USA, [3]Global Monitoring Division, Earth System Research Laboratory, National Oceanic and Atmospheric Administration, Boulder, CO, USA, [4]Department of Atmospheric and Oceanic Sciences, University of Colorado, Boulder, CO, USA, [5]Scripps Institution of Oceanography, University of California, La Jolla, CA, USA, [6]Max Planck Institute, Jena, Germany

Abstract The Southern Annular Mode (SAM) is the dominant mode of climate variability in the Southern Ocean, but only a few observational studies have linked variability in SAM to changes in ocean circulation. Atmospheric potential oxygen (APO) combines atmospheric O_2/N_2 and CO_2 data to mask the influence of terrestrial exchanges, yielding a tracer that is sensitive mainly to ocean circulation and biogeochemistry. We show that observed wintertime anomalies of APO are significantly correlated to SAM in 25- to 30-year time series at three Southern Hemisphere sites, while CO_2 anomalies are also weakly correlated. We find additional correlations between SAM and O_2 air-sea fluxes in austral winter inferred from both an atmospheric inversion of observed APO and a forced ocean biogeochemistry model simulation. The model results indicate that the correlation with SAM is mechanistically linked to stronger wind speeds and upwelling, which brings oxygen-depleted deep waters to the surface.

Plain Language Summary The Southern Annular Mode (SAM) is characterized by variability in the strength of the westerly winds that encircle Antarctica. A more positive SAM index is associated with stronger westerly winds over the ocean at about 60°S latitude. Previous studies based mostly on model simulations have suggested that a positive SAM index is also associated with enhanced upwelling of carbon-rich waters in the Southern Ocean, which influences the uptake and/or release of carbon dioxide to the atmosphere. The same deep waters that have high carbon also have low concentrations of dissolved oxygen, which can cause subtle variations in atmospheric oxygen levels measured at surface stations. We present an analysis of data sets from three Southern Hemisphere stations where air samples have been collected for 25–30 years. We find that during the Southern Hemisphere winter, anomalies in the atmospheric oxygen record are correlated to the SAM index; we find weaker correlations between anomalies in atmospheric carbon dioxide and the SAM index. These results are consistent with variability in air-sea oxygen fluxes from a model simulation. The model results indicate that the observed relationship between SAM and air-sea oxygen fluxes is due to both stronger wind speeds and increased upwelling of oxygen-depleted deep waters.

Key Points:
- Significant correlations are found between winter atmospheric potential oxygen and the Southern Annular Mode at three long-term observing sites
- A similar relationship between winter air-sea O_2 flux and SAM is found in APO inversion products and a hindcast ocean model simulation
- Ocean model simulations indicate that negative winter APO anomalies are linked to stronger wind speeds and ventilation of O_2-depleted deep water

Supporting Information:
- Supporting Information S1

Correspondence to:
C. D. Nevison,
cynthia.nevison@colorado.edu

Citation:
Nevison, C. D., Munro, D. R., Lovenduski, N. S., Keeling, R. F., Manizza, M., Morgan, E. J., & Rödenbeck, C. (2020). Southern Annular Mode influence on wintertime ventilation of the Southern Ocean detected in atmospheric O_2 and CO_2 measurements. *Geophysical Research Letters*, *47*, e2019GL085667. https://doi.org/10.1029/2019GL085667

Received 2 OCT 2019
Accepted 3 FEB 2020
Accepted article online 5 FEB 2020

1. Introduction

The Southern Ocean is a key element of the global climate system (Rintoul, 2018; Sigman et al., 2010). First, it drives the global thermohaline circulation by circumpolar wind-driven upwelling (Marshall & Speer, 2012) and contributes to deep water formation (Haine et al., 1998; Orsi et al., 1999). Second, it supplies macronutrients to the thermocline of the lower latitudes (Moore et al., 2018; Sarmiento et al., 2004) representing an important control on biological productivity of the global oceans. Third, it absorbs ~40% of atmospheric CO_2 of anthropogenic origin (Gruber et al., 2019) mitigating the warming effect caused by CO_2 due to fossil fuel emissions. Understanding how the Southern Ocean will respond to ongoing anthropogenic perturbations is critical for predicting Earth's future climate over the next century and beyond.

Variations in both physical and biogeochemical processes in the Southern Ocean are influenced at interannual to decadal time scales by the changes in wind stress intensity associated with variability in the Southern Annular Mode (SAM; Thompson & Solomon, 2002). When the SAM is in a positive (negative) phase,

westerly winds circling Antarctica intensify (weaken) with the greatest anomalies occurring at approximately 60°S (Thompson & Solomon, 2002). Studies relying mostly on ocean physical-biogeochemical models suggest that periods of positive SAM index are also associated with increased wind-driven upwelling of carbon-rich deep water to the surface, leading to a weakening of net uptake of CO_2 from the atmosphere (Hauck et al., 2013; Le Quéré et al., 2007; Lovenduski et al., 2007).

Recent literature has shown that interannual variability in air-sea CO_2 exchange is marked by contrasting changes in the atmosphere and ocean in different sectors of the Southern Ocean, indicating that the relationship between the SAM index and CO_2 upwelling may be more complex than previously thought (e.g., Landschützer et al., 2015; Gray et al., 2018; DeVries et al., 2017; Landschützer et al., 2019; Keppler & Landschützer, 2019). This literature highlights a debate about the magnitude, driving mechanisms, and even the sign of air-sea CO_2 fluxes in the Southern Ocean. One reason for the debate is the sparse observational network for carbon (and oxygen) measurements in the Southern Ocean (e.g., Bakker et al., 2016; Hauri et al., 2015; Munro et al., 2015). Ship-based observations of the partial pressure of CO_2 (pCO_2) are particularly lacking during winter. While year-round pCO_2 estimates based on new float-based measurements recently have become available, these have higher uncertainty than ship-based observations (Gray et al., 2018; Williams et al., 2017).

Studies of O_2 can provide an important test of our understanding of SAM impacts on the Southern Ocean. Deep waters that are rich in CO_2 are also deficient in dissolved O_2. Therefore, the weakening of CO_2 uptake associated with positive SAM is expected to be associated with strengthening of O_2 uptake from the atmosphere. The air-sea O_2 fluxes at high latitudes are known to be highly seasonal, with O_2 ingassing in winter and outgassing in summer (Garcia & Keeling, 2001; Manizza et al., 2012). We thus may expect the strongest SAM impacts to occur in winter, when wind-driven upwelling and surface cooling reach their peak, bringing the most O_2-deficient waters to the surface. However, despite some progress in tracking changes in Southern Ocean dissolved O_2 (Bushinsky et al., 2017), the historical coverage in dissolved O_2 measurements, as with ocean pCO_2, is still too sparse to reliably resolve SAM signals.

Long-term, continuous measurements of atmospheric CO_2 and O_2 provide an alternative perspective on seasonal and interannual variability in ocean biogeochemistry. Atmospheric O_2 and CO_2 have been measured for 25 to 30 years at several surface monitoring sites in the Southern Ocean. They can be combined to define a unique tracer, atmospheric potential oxygen (APO ~ O_2/N_2 + 1.1 CO_2), where 1.1 is the approximate O_2:C ratio from land photosynthesis (Severinghaus, 1995). By design, APO largely removes the influence of terrestrial photosynthesis and respiration, which produce effects on O_2 and CO_2 that cancel in APO. Fossil fuel combustion typically has a larger (~1.4) O_2:C ratio and therefore produces changes in O_2 and CO_2 that do not fully cancel and effectively deplete APO (Stephens et al., 1998). APO data have revealed both a long-term decreasing secular trend, the result of fossil fuel combustion and ocean uptake of anthropogenic CO_2, and annually repeating seasonal cycles, which are largest at middle to high latitudes (Battle et al., 2006; Bender et al., 2005; Keeling et al., 1996). These seasonal cycles are driven mainly by the influence of spring/summer outgassing of O_2 due to photosynthetic production in the surface ocean, followed by O_2 ingassing due to fall/winter ventilation of O_2-depleted subsurface waters. In contrast, the corresponding air-sea exchange of CO_2 generally has much weaker seasonality due to the buffering chemistry of CO_2 in seawater (Keeling et al., 1993). Thus, on seasonal and shorter time scales, over which the atmosphere is zonally well mixed, APO data provide a broad-scale, regionally integrated metric of oceanic O_2 gains or losses. Subtle changes in the shape and amplitude of the APO seasonal cycle offer a means of detecting and evaluating interannual variability in ocean circulation and biogeochemistry.

In this paper, we use APO to assess the role of climate variability in Southern Ocean ventilation. We examine interannual anomalies in APO and CO_2 and their correlation to SAM at several long-term monitoring sites in the Southern Hemisphere. We also examine correlations between SAM and the air-sea fluxes of oxygen inferred from an atmospheric inversion of observed APO and predicted by a forced ocean biogeochemistry model simulation. We use the model to explore the mechanisms driving the observed correlations, including higher wind speeds and corresponding stronger wind stress associated with positive SAM, as well as stronger upwelling, which brings more O_2-depleted deep water to the surface.

2. Materials and Methods

2.1. APO and CO_2 Data

Atmospheric O_2/N_2 and CO_2 data from three long-term surface monitoring sites in the Scripps Institution of Oceanography (SIO) network, South Pole (90°S, 24.8°W), Palmer Station, Antarctica (64.9°W, 64.0°W), and Cape Grim, Tasmania (40.7°S, 144.7°E), are available from the early 1990s to mid-1990s, depending on the site (Keeling et al., 1996; Manning & Keeling, 2006). Cryogenically dried samples are collected at 1- to 2-week intervals at 1-atm pressure in triplicate in 5-L glass flasks sealed with Viton O-rings. Our analysis relies on measurements of O_2/N_2 ratio and CO_2 mole fraction in these flasks, measured on an interferometric O_2/N_2 analyzer and a Siemens nondispersive infrared CO_2 analyzer, respectively. We define the APO tracer according to

$$\mathrm{APO} = \delta(\mathrm{O_2/N_2}) + \frac{1.1}{X_{o2}}\mathrm{CO_2}, \tag{1}$$

where $\delta(O_2/N_2)$ is the relative deviation in the O_2/N_2 ratio from a reference ratio in per meg units, $X_{O2} = 0.2094$ is the O_2 mole fraction of dry air (Stephens et al., 1998), CO_2 is the mole fraction of carbon dioxide in parts per million (μmol mol^{-1}), and 1.1 is a representative O_2:C ratio of terrestrial respiration and photosynthesis (Severinghaus, 1995).

2.2. Analysis of Seasonal Anomalies

To compute seasonal anomalies for APO and CO_2 time series we followed a multistep process to account for the irregularity of sampling and remove both the seasonal cycle and long-term trend. First, monthly mean APO and CO_2 time series were computed from the raw quasi-fortnightly time series (Figure S1 in the supporting information). The entire original time series was fit with a third-order polynomial plus first four-harmonic curve (Thoning et al., 1989). Following Hamme and Keeling (2008), monthly averages were determined by adjusting each APO and CO_2 data point to the 15th of its month by "sliding" it parallel to the polynomial and four-harmonic fit; the average for the month was computed (i.e., in months with more than one measurement, the average was taken of all adjusted mid-month data points). This approach yielded similar results to using the simple monthly mean of all data points collected in a given month and year. The adjusted monthly mean data were detrended with a third-order polynomial. A climatological seasonal cycle with monthly resolution was constructed by taking the average of the detrended data for all Januaries, Februaries, etc. The climatological cycle was subtracted from the original raw data to produce a deseasonalized but not detrended curve. A running annual mean (effectively a 13-month running mean centered on the month of interest) then was computed for the purpose of removing the secular trend and other low-frequency variability. At stations with gaps in the monthly data, the original third-order polynomial fit was used as a placeholder in the running mean. The running mean was subtracted from the deseasonalized curve to isolate the residual high-frequency anomalies. These high-frequency residuals were sorted by month and plotted against smoothed SAM anomalies from http://www.cpc.ncep.noaa.gov/ from the corresponding month and year. A 4-month filter (effectively a 5-month running mean centered on the month of interest) was applied to the SAM anomalies for the purpose of smoothing out their strong month-to-month variability. For each month, a least-squares linear regression was performed on the APO or CO_2 monthly residual versus SAM scatterplots. The different steps of this methodology are illustrated for the APO time series at Palmer Station in Figures S1 and S2. The correlations coefficients and p values were computed in MATLAB with the assumption that a p value < 0.05 was statistically significant at the 95% confidence level while a p value < 0.1 was marginally significant at the 90% confidence level. Various sensitivity tests were performed, including lagging the SAM index several months before and after the APO and CO_2 anomalies and using variable time lengths of both the APO low-pass filter and the SAM smoother.

2.3. Air-Sea O_2 and CO_2 Fluxes

The same methodology described in section 2.2 was used to compute monthly high-frequency residuals for (a) estimated air-sea APO fluxes from an atmospheric inversion of SIO APO data (Rödenbeck et al., 2008) and (b) monthly mean air-sea O_2 and CO_2 fluxes from an ocean-sea ice "hindcast" simulation of the Community Earth System Model (CESM). For all these fields, the monthly mean fluxes were integrated zonally over 40–60°S and regressed against smoothed monthly SAM anomalies using MATLAB software.

Correlations with $p < 0.05$ were considered significant (95% confidence level), while correlations with $p < 0.1$ were considered marginally significant (90% confidence level).

Sea-air APO fluxes (referred to as fAPO or the Jena inversion fluxes) were estimated from time series of measured APO at seven atmospheric stations of the world-wide SIO network (update of Manning & Keeling, 2006) using an inversion of atmospheric transport (Jena CarboScope run apo97_v1.6, https://www.bgc-jena.mpg.de/CarboScope/, update of Rödenbeck et al., 2008). The inversion determines the spatiotemporal APO flux field that leads to the best match between APO simulated by an atmospheric transport model (driven by reanalyzed meteorological fields) and the APO measurements. Bayesian a priori constraints are used to regularize the estimation, which otherwise would be highly underdetermined. These a priori constraints guide seasonal APO flux variability toward areas of larger seasonal cycles in the Garcia and Keeling (2001) oxygen flux climatology but allow interannual variations equally in any part of the ocean.

The CESM fields are referred to as fO_2 and fCO_2 and are air-sea fluxes (not atmospheric mixing ratios) from a hindcast simulation forced with observed and reanalyzed momentum, heat, and freshwater fluxes from 1979–2017 (Lovenduski et al., 2019; Yeager et al., 2018) (we note that previous work, which used an atmospheric transport model to convert CESM air-sea fluxes into APO fields, found good agreement between modeled and observed APO seasonal cycles over the Southern Ocean [Nevison et al., 2016]). The CESM ocean model resolution on its native off-polar grid was ~1° latitude by 1.125° longitude, with 60 depth levels including 10-m depth resolution in the upper ocean. The native fields were interpolated to a regular 1° × 1° latitude/longitude grid using Climate Data Operators freeware (https://code.zmaw.de/projects/cdo). In addition to the 40–60°S zonal integrals described above, spatially variable (i.e., resolved at each model grid point) regressions against monthly SAM anomalies were calculated using NCAR Command Language (NCL) software (https://www.ncl.ucar.edu/). Statistical significance was estimated by comparing the NCL correlation coefficients to critical R values determined from a t table (Sokal & Rohlf, 1981). For the 39-year model run ($N - 2 = 37$), $R_{crit} = 0.315$ (95% confidence level) and 0.267 (90% confidence level).

2.4. Analysis of Forcing Mechanisms Using CESM Output

Mechanistic forcing of interannual variability in fO_2 was investigated using CESM by separating the contributions due to variability in the piston velocity (K) and the saturation state of dissolved O_2 (i.e., $O_2 - O_{2sat}$), which together determine fO_2:

$$fO_2 = K[O_2\text{–}O_{2sat}] = \overline{K}[O_2\text{–}O_{2sat}] + K\overline{[O_2 - O_{2sat}]} + \text{residual}, \quad (2)$$

where the horizontal bar indicates the mean climatological seasonal cycle and $\overline{K}[O_2\text{–}O_{2sat}]$ and $K\overline{[O_2 - O_{2sat}]}$ are the fO_2 fluxes for which interannual variability is determined only by the $[O_2 - O_{2sat}]$ or K terms, respectively. The correlations of the separated fO_2 terms versus SAM were computed as described 2.3 below in order to estimate the relative contribution of each term in driving the correlation.

3. Results

We find that the August APO anomaly at Palmer Station is negatively correlated ($R = 0.57$, $p = 0.01$) with the SAM index (Figure 1). At Palmer Station, a significant negative correlation is also found for the July and August average ($R = 0.56$, $p = 0.01$), and a marginally significant negative correlation is found for the month of July alone ($R = 0.38$, $p = 0.10$). These months correspond to the period of strong ventilation within the Southern Ocean when APO is descending to its wintertime minimum, which typically occurs in September. A similar negative correlation is found between APO and SAM at Cape Grim ($R = 0.55$, $p = 0.01$) for July and August (Figure S4) and at South Pole ($R = 0.58$, $p = 0.01$), where the correlation is evident only in August (Figure S5). We also find positive correlations between the CO_2 anomaly and the SAM index at Palmer Station for August ($R = 0.45$, $p = 0.05$) and for the July and August average ($R = 0.39$, $p = 0.10$). At South Pole we find a positive correlation between the CO_2 anomaly and SAM in August ($R = 0.38$, $p = 0.07$), but we find no significant correlations between CO_2 and SAM at Cape Grim (Figures S4 and S5).

The correlations at Palmer Station are similar but strengthened when a longer filter (e.g., a 25- or 37-month centered running mean) is used to remove low-frequency variability from the APO and CO_2 time series. However, a 13-month centered running mean is used as the default to preserve as long a time series as

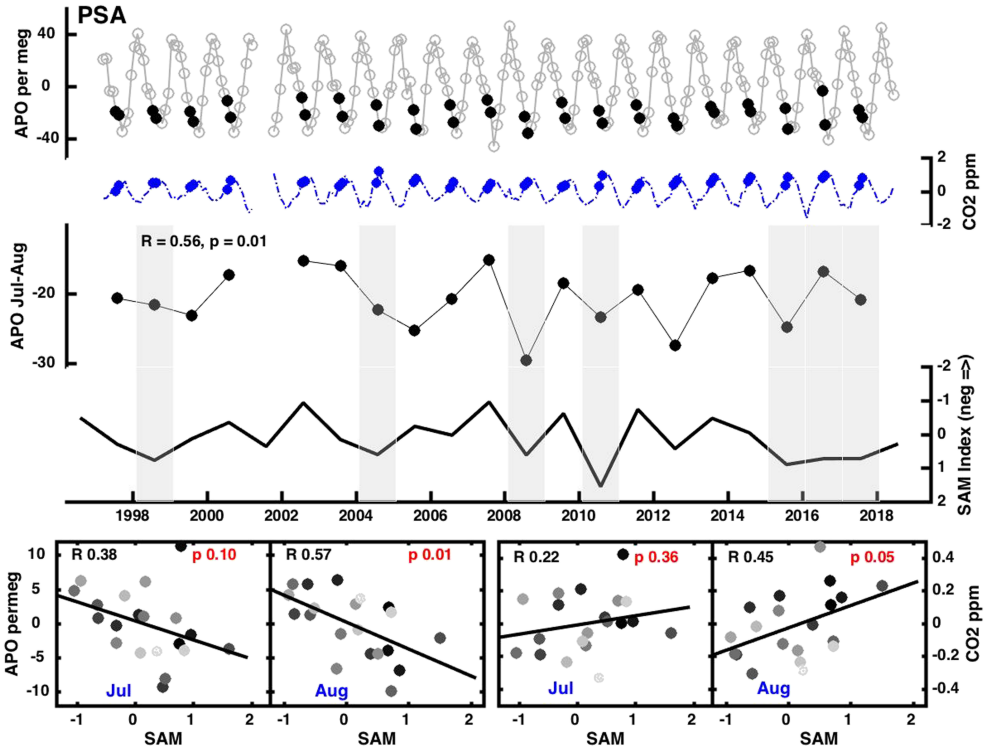

Figure 1. Top panels: detrended APO (black) and CO_2 (blue) observed at Palmer Station, Antarctica, with July and August filled in as solid symbols. Middle panels: time series illustrating the negative correlation between SAM and wintertime (mean July and August) APO anomalies. Gray bands denote periods when the July and August 4-month smoothed SAM index is >0.5. Bottom panels: monthly scatterplots of APO anomalies versus SAM (left) and atmospheric CO_2 anomalies versus SAM (right), plotted for each of July and August. The anomalies are plotted with a shaded gray scale, where dark colors indicate the most recent years and light colors indicate the oldest years in the record.

possible for the comparison to SAM, since the running mean truncates the time series at both ends by half the filter length. The correlations are also similar when a 2-month or 6-month (rather than the default 4-month) smoothing routine is applied to the SAM anomalies but weaken substantially using an 8-month or longer smoothing interval. The lagged analysis suggests that the correlations between APO and SAM are strongest when centered directly on August but are still significant when the (4-month smoothed) SAM index is lagged by ±2 months. In contrast, the correlation with August atmospheric CO_2 is strongest when the SAM index is lagged 1 and 2 months prior (i.e., to June or July [$R = 0.52$]) rather than centered on August ($R = 0.45$). August CO_2 is not significantly correlated to SAM indices lagged later than August.

In the Jena inversion, the fAPO product is negatively correlated with SAM ($R = 0.62$, $p = 0.005$), when averaged over 40–60°S during July and August, a time when fAPO is at its maximum negative value (maximum invasion of O_2) (Figure 2, top panel). The fAPO versus SAM correlation is evident in both months, although slightly stronger in July ($R = 0.57$, $p = 0.01$) than August ($R = 0.48$, $p = 0.04$) (Figure 2, lower left panels).

The CESM model results show a similar negative correlation between SAM and the air-sea O_2 flux (Figure 2, middle and lower right panels), although the correlation occurs only for July ($R = 0.64$, $p = 0.001$), not August. The zonally averaged CESM air-sea CO_2 flux is not correlated to SAM in austral winter, although it appears weakly correlated in October ($R = 0.39$, $p = 0.09$). An analysis of the spatial structure of the July CESM fO_2 versus SAM correlation shows that the strongest correlations are centered in the Pacific sector of the Southern Ocean between about 100°W and 150°W and in the Indian sector between 60°E and 150°E (Figure 3, left panel). A similar correlation in these regions is apparent in July between SAM and the CESM ideal age of water (IAGE) tracer at a depth of 45 m, where IAGE is the number of years since the water parcel was last in contact with the surface (Figure 3, right panel).

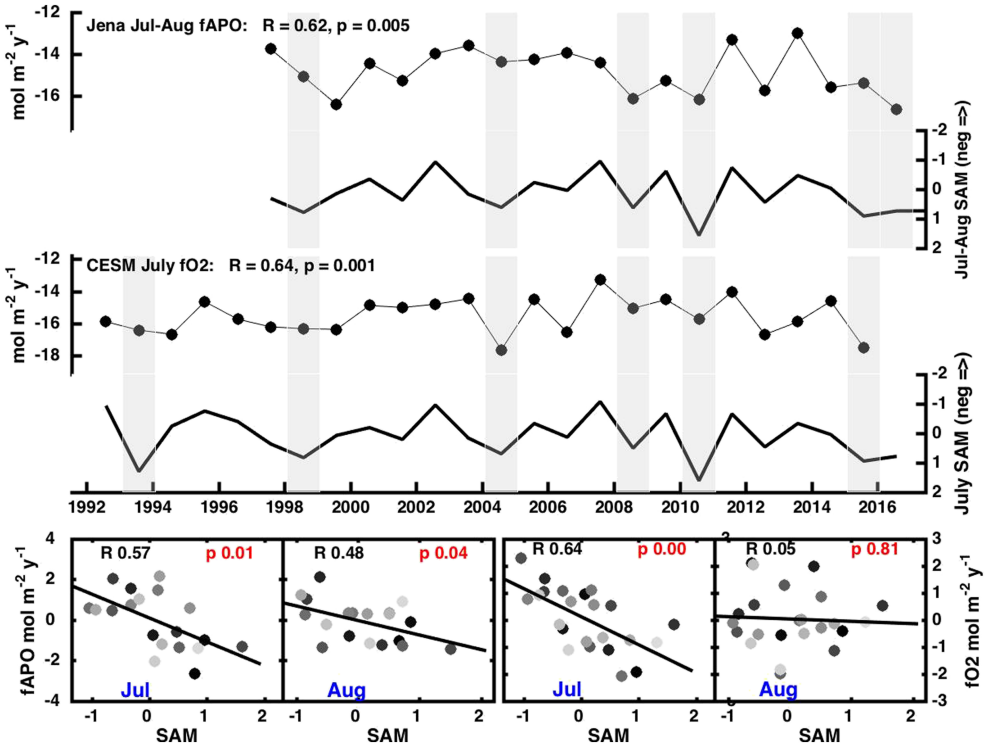

Figure 2. Top panels: time series illustrating the correlation between positive SAM and wintertime fAPO from the Jena inversion product zonally integrated from 40–60°S and averaged over July and August. Middle panels: time series illustrating the correlation between SAM and the July air-sea O_2 flux from the forced CESM run zonally integrated from 40–60°S. Gray bands denote periods when the 4-month smoothed SAM index is >0.5. Bottom panels: monthly scatterplots of Jena fAPO anomalies versus SAM (left) and CESM fO_2 anomalies versus SAM (right), plotted for each of July and August. The anomalies are plotted with a shaded gray scale, where dark colors indicate the most recent years and light colors indicate the oldest years in the record.

Coherent relationships for July using CESM output were also observed between SAM and piston velocity (K), mixed layer depth (Figure S6), SST, heat flux, and sea-level pressure (not shown). K shows the most widespread positive correlations with SAM especially throughout the Pacific Ocean and Indian Ocean sectors of the Southern Ocean (Figure S6). A separation analysis indicates that variability in K dominates the zonally averaged (40–60°S) fO_2 versus SAM signal, contributing about 65% of the observed signal as compared with about 35% for the $(O_2 - O_{2sat})$ term. However, within the Pacific patch where the strongest correlation between fO_2 and SAM is observed, the $(O_2 - O_{2sat})$ term contributes up to 80% of the observed variability (Figure S7). The residual term in equation (2) is generally small in the separation analysis, accounting for about 3% of the observed variability.

4. Discussion

Our study uniquely links variability in APO observed at Southern Hemisphere surface stations to SAM. While previous studies have hypothesized coherent variability between SAM and air-sea trace gas fluxes, these studies have relied heavily on models and focused on CO_2 (e.g., Le Quéré et al., 2007; Lovenduski et al., 2007). However, atmospheric CO_2, unlike APO, has strong influences from the land biosphere in the Southern Hemisphere (figure 16 in Heimann et al., 1989). In the current analysis, we show that three multidecadal APO records from stations in the middle and high southern latitudes are correlated with SAM in austral winter, the season when variability in APO mainly reflects ventilation of O_2-depleted deep waters.

We also observe austral winter variability in atmospheric CO_2 that is consistent with enhanced ventilation of CO_2-enriched deep waters during positive SAM. However, these correlations are weak compared to the APO

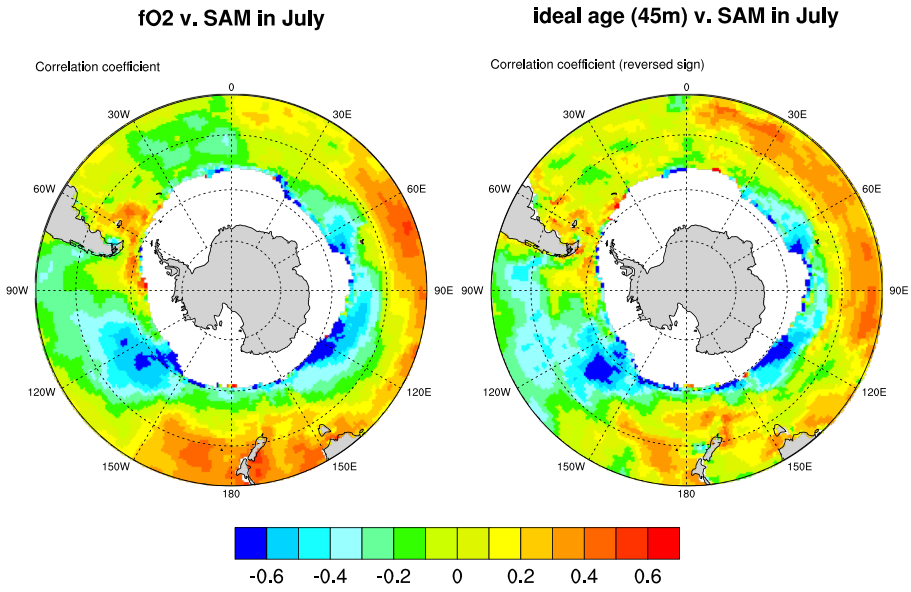

Figure 3. Spatially resolved correlation coefficients (left panels) for July anomalies from CESM regressed against the SAM index. Left panel: air-sea O_2 flux versus SAM. Right panel: ideal age at 45 m (in the winter mixed layer) versus SAM. Note that the sign of the ideal age correlation coefficient is reversed to facilitate comparison with the fO_2 correlation coefficient. In both panels, white areas are covered by sea ice in July.

versus SAM correlations and are evident mainly at Palmer Station and South Pole but not Cape Grim. Our CO_2 results are consistent with previous work by Butler et al. (2007), who noted a weak correlation between SAM and atmospheric CO_2 at Palmer Station, and by Lindsay (2016), who found a marginally significant relationship between $^{14}CO_{2atm}$ and SAM based on a near decade-long record from the Drake Passage. In that study, negative $^{14}CO_{2atm}$ associated with upwelling of ^{14}C-depleted deep waters was correlated to positive SAM anomalies. The observed differences in the strength and coherence of the APO correlation with SAM versus the CO_2 correlation with SAM are expected, due to the slower response of the carbonate system to air-sea gas exchange relative to the more rapid air-sea exchange of dissolved O_2.

In theory, a correlation between SAM and APO at Palmer, South Pole, or Cape Grim could arise either due to variations in air-sea APO flux tied to SAM or due to SAM-related changes in atmospheric circulation, bringing air of different origins to each station. Evidence that the APO variations are at least partly driven by air-sea APO flux is found in the atmospheric APO inversion, which accounts in principle for the circulation influence and still yields fAPO estimates that are negatively correlated with SAM during peak invasion of O_2 in austral winter (Figure 2).

The relationship with SAM detected in fO_2 from a CESM hindcast simulation provides mechanistic insight into the atmospheric data and the inversion results described above. First, it is noteworthy that both the CESM fO_2 and Jena fAPO versus SAM correlations are strongest 0.5–1 month earlier than the APO versus SAM correlations, which is consistent with a time lag associated with transport of the atmospheric signal to the sampling station. In CESM, we find that SAM influences fO_2 through both K, which is dependent on wind speed, and through upwelling of O_2-depleted deep waters. The CESM hindcast tracer of water mass age, IAGE, provides further evidence that mixing of older water to the surface occurs during intervals of positive SAM, consistent with enhanced ventilation.

A spatial analysis of the CESM hindcast fO_2 and IAGE tracers (Figure 3), as well as of other parameters tied to wind speed and upwelling (Figures S6 and S7), suggests substantial regional differences. In CESM, the imprint of O_2-depleted deep waters during periods of positive SAM is most evident in subregions of the Pacific and Indian sectors of the Southern Ocean (Figure 3). Interestingly, recent analyses of the relationship between SAM and pCO_2 (Keppler & Landschützer, 2019) and between SAM and mixed layer depth (Sallée et al., 2012) found a similar regional asymmetry in the ocean's response to SAM, with the strongest response concentrated in the Pacific sector of the Southern Ocean.

The APO results are potentially relevant for recent studies that have documented previously unrecognized strong interannual and decadal variability in ocean pCO_2 and air-sea CO_2 flux in the Southern Ocean (e.g., Verdy et al., 2007; Landschützer et al., 2015). These studies have suggested that this variability may be related to climate modes other than SAM, since the variability is regionally heterogeneous in ways that are not well described by SAM (e.g., Keppler & Landschützer, 2019). Our results provide observational confirmation of the mechanism indicated by earlier model-based studies; that is, that enhanced upwelling during years of positive SAM influences the air-sea flux of dissolved ocean tracers like CO_2 and O_2 that have strong depth gradients. However, our spatially resolved CESM results also support the more recent studies in suggesting a highly heterogeneous regional response to SAM. Furthermore, our APO and air-sea O_2 flux correlations with SAM are stronger than those involving CO_2, which could reflect the damping influence of carbonate chemistry or could also indicate a more complex relationship between CO_2 and SAM.

5. Conclusions

Multidecadal APO records from long-term monitoring sites at Palmer Station, Antarctica, Cape Grim, Tasmania, and South Pole, Antarctica, are negatively correlated with SAM in austral winter months. Results from the Jena APO inversion indicate that this correlation is partly the result of large-scale variations in fAPO, which is dominated by the air-sea flux of O_2. The CESM ocean model reproduces the austral winter correlation between air-sea O_2 fluxes and SAM and offers the mechanistic insight that the influences of SAM on the piston velocity and on surface O_2 saturation state are both important contributors to the correlation.

Acknowledgments

C. D. N., D. R. M., and N. S. L. thank NASA Ocean Biology and Biogeochemistry Award NNX16AT52G. We thank Matt Long and Keith Lindsay of NCAR for the help in interpreting CESM forced run output. We also thank two anonymousreviewers for their helpful comments, which much improved the manuscript. The Decadal Prediction Large Ensemble CESM output analyzed in this paper represents monthly output from the forced ocean and sea ice simulation and is accessible at http://www.cesm.ucar.edu/projects/community-projects/DPLE/. The SIO APO and CO_2 output is available at http://scrippso2.ucsd.edu and http://scrippsco2.ucsd.edu. We thank NSF for support for sample collection at Palmer Station and South Pole, and the AustralianBureau of Meteorology for sample collections at Cape Grim Observatory. Measurements of O_2/N_2 and CO_2 from the Scripps O_2 program have been supported by a series of grants from the U.S. National Science Foundation and the National Oceanographic and Atmospheric Administration and, most recently, from NOAA Grant NA15OAR4320071. Any opinions, findings, and conclusions or recommendations expressed in this material are those of the authors and do not necessarily reflect the views of NSF and NOAA. The Jena fAPO inversion products are available from http://www.bgc-jena.mpg.de/CarboScope/. The SAM anomalies are available from http://www.cpc.ncep.noaa.gov/and are listed under AAO (Antarctic Oscillation) rather than SAM.

References

Bakker, D. C. E., Pfeil, B., Landa, C. S., Metzl, N., O'Brien, K. M., Olsen, A., et al. (2016). A multi-decade record of high-quality fCO_2 data in version 3 of the Surface Ocean CO_2 Atlas (SOCAT). *Earth System Science Data*, *8*, 297–323. https://doi.org/10.5194/essd-2016-15

Battle, M., Mikaloff Fletcher, S., Bender, M. L., Keeling, R. F., Manning, A. C., Gruber, N., et al. (2006). Atmospheric potential oxygen: New observations and their implications for some atmospheric and oceanic models. *Global Biogeochemical Cycles*, *20*, GB1010. https://doi.org/10.1029/2005GB002534.

Bender, M., Ho, D., Hendricks, M. B., Mika, R., Battle, M. O., Tans, P., et al. (2005). Atmospheric O_2/N_2 changes, 1993–2002: Implications for the partitioning of fossil fuel CO_2 sequestration. *Global Biogeochemical Cycles*, *19*, GB4017. https://doi.org/10.1029/2004GB002410

Bushinsky, S. M., Gray, A. R., Johnson, K. S., & Sarmiento, J. L. (2017). Oxygen in the Southern Ocean from Argo floats: Determination of processes driving air-sea fluxes. *Journal of Geophysical Research, Oceans*, *122*, 8661–8682.

Butler, A. H., Thompson, D. W. J., & Gurney, K. R. (2007). Observed relationships between the Southern Annular Mode and atmospheric carbon dioxide. *Global Biogeochemical Cycles*, *21*, GB4014. https://doi.org/10.1029/2006GB002796

DeVries, T., Holzer, M., & Primeau, F. (2017). Recent increase in oceanic carbon uptake driven by weaker upper-ocean overturning. *Nature*, *542*(7640), 215–218. https://doi.org/10.1038/nature21068

Garcia, H. E., & Keeling, R. F. (2001). On the global oxygen anomaly and air-sea flux. *Journal of Geophysical Research*, *106*(C12), 31,155–31,166. https://doi.org/10.1029/1999JC000200

Gray, A., Johnson, K. S., Bushinsky, S. M., Riser, S. C., Russell, J. L., Talley, L. D., et al. (2018). Autonomous biogeochemical floats detect significant carbon dioxide outgassing in the high-latitude Southern Ocean. *Geophysical Research Letters*, *45*, 9049–9057. https://doi.org/10.1029/2018GL078013

Gruber, N., Landschutzer, P., & Lovenduski, N. S. (2019). The variable Southern Ocean carbon sink. *Annual Review of Marine Science*, *11*, 159–186. https://doi.org/10.1146/annurev-marine-121916-063407

Haine, T. W. N., Watson, A. J., Liddicoat, M. I., & Dickson, R. R. (1998). The flow of Antarctic bottom water to the southwest Indian Ocean estimated using CFCs. *Journal of Geophysical Research*, *103*(C12), 27,637–27,653.

Hamme, R., & Keeling, R. F. (2008). Ocean ventilation as a driver of interannual variability in atmospheric potential oxygen. *Tellus*, *60B*. https://doi.org/10.1111/j.1600-0889.2008.00376.x

Hauck, J., Völker, C., Wang, T., Hoppema, M., Losch, M., & Wolf-Gladrow, D. A. (2013). Seasonally different carbon flux changes in the Southern Ocean in response to the Southern Annular Mode. *Global Biogeochemical Cycles*, *27*(4), 1236–1245. https://doi.org/10.1002/2013GB004600

Hauri, C., Doney, S. C., Takahashi, T., Erickson, M., Jiang, G., & Ducklow, H. W. (2015). Two decades of inorganic carbon dynamics along the West Antarctic Peninsula. *Biogeosciences*. https://doi.org/10.5194/bg-12-6761-2015

Heimann, M., Keeling, C. D. , & Tucker, C. J. (1989). In D. H. Peterson (Eds.), *Aspects of Climate Variability in the Pacific and the Western Americas* (pp. 277–303). Washington, DC: American Geophysical Union.

Keeling, R. F., Najjar, R. G., Bender, M. L., & Tans, P. P. (1993). What atmospheric oxygen measurements can tell us about the global carbon cycle. *Global Biogeochemical Cycles*, *7*, 37–67.

Keeling, R. F., Piper, S. C., & Heimann, M. (1996). Global and hemispheric CO_2 sinks deduced from changes in atmospheric O_2 concentration. *Nature*, *391*, 218–221.

Keppler, L., & Landschützer, P. (2019). Regional wind variability modulates the Southern Ocean carbon sink. *Scientific Reports*, *9*(1), 7384. https://doi.org/10.1038/s41598-019-43826-y

Landschützer, P., Gruber, N., Haumann, F. A., Rödenbeck, C., Bakker, D. C. E., van Heuven, S., Hoppema, M., et al. (2015). The reinvigoration of the Southern Ocean carbon sink. *Science*, *349*, 1221–1224.

Landschützer, P., Ilyina, T., & Lovenduski, N. S. (2019). Detecting regional modes of variability in observation-based surface ocean pCO_2. *Geophysical Research Letters*. https://doi.org/10.1029/2018GL081756

Le Quéré, C., Rödenbeck, C., Buitenhuis, E. T., Conway, T. J., Langenfelds, R., Gomez, A., et al. (2007). Saturation of the Southern Ocean CO_2 sink due to recent climate change. *Science*, *316*(5832), 1735–1738. https://doi.org/10.1126/science.1136188

Lindsay, C. (2016). Carbon dynamics of the deglacial and contemporary ocean inferred from radiocarbon measurements in foraminifera, seawater and atmospheric carbon dioxide. University of Colorado Boulder, PhD.

Lovenduski, N. S., Gruber, N., Doney, S. C., & Lima, I. D. (2007). Enhanced CO_2 outgassing in the Southern Ocean from a positive phase of the Southern Annular Mode, Global Biogeochem. *Cycle*, *21*, GB2026. https://doi.org/10.1029/2006GB002900

Lovenduski, N. S., Yeager, S. G., Lindsay, K., & Long, M. C. (2019). Predicting near-term variability in ocean carbon uptake. *Earth System Dynamics*, *10*(45–57), 2019. https://doi.org/10.5194/esd-10-45-2019

Manizza, M., Keeling, R. F., & Nevison, C. D. (2012). On the processes controlling the seasonal cycles of the air-sea fluxes of O_2 and N_2O: A modeling study. *Tellus-B*, *64*(1), 18429. https://doi.org/10.3402/tellusb.v64i0.18429

Manning, A. C., & Keeling, R. F. (2006). Global oceanic and land biotic carbon sinks from the Scripps atmospheric oxygen flask sampling network. *Tellus-B*, *58B*, 95–116.

Marshall, J., & Speer, K. (2012). Closure of the meridional overturning circulation through Southern Ocean circulation. *Nature Geoscience*, *5*, 171–180.

Moore, J. K., Fu, W., Primeau, F., Britten, G. L., Lindsay, K., Long, M., et al. (2018). Sustained climate warming drives declining marine biological productivity. *Science*, *359*(6380), 1139–1143. https://doi.org/10.1126/science.aao6379

Munro, D. R., Lovenduski, N. S., Takahashi, T., Stephens, B. B., Newberger, T., & Sweeney, C. (2015). Recent evidence for a strengthening CO_2 sink in the Southern Ocean from carbonate system measurements in the Drake Passage (2002–2015). *Geophysical Research Letters*, *42*, 7623–7630. https://doi.org/10.1002/2015GL065194

Nevison, C. D., Manizza, M., Keeling, R. F., Stephens, B. B., Bent, J. D., Dunne, J., et al., et al. (2016). Evaluating CMIP5 ocean biogeochemistry and Southern Ocean carbon uptake using atmospheric potential oxygen: Present-day performance and future projection. *Geophysical Research Letters*, *43*, 2077–2085. https://doi.org/10.1002/2015GL067584

Orsi, A. H., Johnson, G. C., & Bullister, J. L. (1999). Circulation, mixing, and production of Antarctic bottom water. *Progress in Oceanography*, *43*, 55–109.

Rintoul, S. (2018). The global influence of localized dynamics in the Southern Ocean. *Nature*, *558*(7709), 209–218. https://doi.org/10.1038/s41586-018-0182-3

Rödenbeck, C., Le Quéré, C., Heimann, M., & Keeling, R. F. (2008). Interannual variability in oceanic biogeochemical processes inferred by inversion of atmospheric O_2/N_2 and CO_2 data. *Tellus B*, *60*, 685–705.

Sallée, J.-B., Matear, R. J., Rintoul, S. R., & Lenton, A. (2012). Localized subduction of anthropogenic carbon dioxide in the Southern Hemisphere oceans. *Nature Geoscience*, *5*, 579–584.

Sarmiento, J. L., Gruber, N., Brzezinski, M. A., & Dunne, J. P. (2004). High-latitude controls of thermocline nutrients and low latitude biological productivity. *Nature*, *427*, 56–60.

Severinghaus, J. W. (1995). Seeking bottom lines in the deeper oxygen picture. *Acta Anaesthesiologica Scandinavica*, *39*, 47–51.

Sigman, D. M., Hain, M. P., & Haug, G. H. (2010). The polar ocean and glacial cycles in atmospheric CO_2 concentration. *Nature*, *466*, 47–55.

Sokal, R. R., & Rohlf, F. J. (1981). *Biometry* (p. 859). New York: W.H. Freeman.

Stephens, B. B., Keeling, R. F., Heimann, M., Six, K. D., Murnane, R., & Caldeira, K. (1998). Testing global ocean carbon cycle models using measurements of atmospheric O_2 and CO_2 concentration, Global Biogeochem. *Cycle*, *12*, 213–230.

Thompson, D. W. J., & Solomon, S. (2002). Interpretation of recent Southern Hemisphere climate change. *Science*, *296*(5569), 895–899. https://doi.org/10.1126/science.1069270

Thoning, K. W., Tans, P. P., & Komhyr, W. D. (1989). Atmospheric carbon dioxide at Mauna Loa Observatory: 2. Analysis of the NOAA GMCC data, 1974–1985. *Journal of Geophysical Research*, *94*, 8549–8565.

Verdy, A., Dutkiewicz, S., Follows, M. J., Marshall, J., & Czaja, A. (2007). Carbon dioxide and oxygen fluxes in the Southern Ocean: Mechanisms of interannual variability. *Global Biogeochemical Cycles*, *21*, GB2020. https://doi.org/10.1029/2006GB002916

Williams, N. L., Juranek, L. W., Feely, R. A., Johnson, K. S., Sarmiento, J. L., Talley, L. D., et al. (2017). Calculating surface ocean pCO_2 from biogeochemical Argo floats equipped with pH: An uncertainty analysis. *Global Biogeochemical Cycles*, *31*(3), 591–604. https://doi.org/10.1002/2016GB005541

Yeager, S. G., Danabasoglu, G., Rosenbloom, N. A., Strand, W., Bates, S. C., Meehl, G. A., et al. (2018). Predicting near-term changes in the Earth system: A large ensemble of initialized decadal prediction simulations using the Community Earth System Model. *BAMS*, *99*(9), 1867–1886. https://doi.org/10.1175/BAMS-D-17-0098.1